

Multi-conjugated adaptive optics imaging of distant galaxies – A comparison of Gemini/GSAOI and VLT/HAWK-I data

Mischa Schirmer^{1*}, Vincent Garrel^{1,2}, Gaetano Sivo¹, Eduardo Marin¹
and Eleazar R. Carrasco¹

¹*Gemini Observatory, Casilla 603, La Serena, Chile*

²*Max-Planck-Institut für extraterrestrische Physik, 85748 Garching, Germany*

Accepted XXX. Received YYY; in original form ZZZ

ABSTRACT

Multi-conjugated adaptive optics (MCAO) yield nearly diffraction-limited images at $2\ \mu\text{m}$ wavelengths. Currently, GeMS/GSAOI at Gemini South is the only MCAO facility instrument at an 8m telescope. Using real data and for the first time, we investigate the gain in depth and S/N when MCAO is employed for K_s -band observations of distant galaxies. Our analysis is based on the *Frontier Fields* cluster MACS J0416.1–2403, observed with GeMS/GSAOI (near diffraction-limited) and compared against VLT/HAWK-I (natural seeing) data. Using galaxy number counts, we show that the substantially increased thermal background and lower optical throughput of the MCAO unit are fully compensated for by the wavefront correction, because the galaxy images can be measured in smaller apertures with less sky noise. We also performed a direct comparison of the signal-to-noise ratios (S/N) of sources detected in both data sets. For objects with intrinsic angular sizes corresponding to half the HAWK-I image seeing, the gain in S/N is 40 per cent. Even smaller objects experience a boost in S/N by a up to a factor of 2.5 despite our suboptimal natural guide star configuration. The depth of the near diffraction limited images is more difficult to quantify than that of seeing limited images, due to a strong dependence on the intrinsic source profiles. Our results emphasize the importance of cooled MCAO systems for K_s -band observations with future, extremely large telescopes.

Key words: instrumentation: adaptive optics, galaxies: clusters: individual: MACS J0416.1–2403

1 INTRODUCTION

Atmospheric turbulence reduces the depth and resolution of ground-based imaging. Multi-conjugated adaptive optics (MCAO, see Ragazzoni et al. 2000; Ellerbroek & Rigaut 2000) compensates the wavefront distortion and reduces plate-scale dynamical distortions by using information from several natural guide stars (NGS) as well as laser guide stars (LGS). The corrections are sent to two or more deformable mirrors conjugated to different altitudes. Nearly diffraction-limited images can be achieved over arcminute scales in the near-infrared (NIR).

A MCAO demonstrator (MAD) was installed at the Very Large Telescope (VLT) for several runs in 2008. A survey of the results is presented by Melnick et al. (2012), highlighting the success of the technology, but also a strong

focus on targets with resolved stellar populations. Results for the two extragalactic observations (COSMOS field, Chandra Deep Field South) have not yet been published.

The completion of the Gemini Multi-Conjugate Adaptive Optics System (GeMS, Rigaut et al. 2014; Neichel et al. 2014b) and the Gemini South Adaptive Optics Imager (GSAOI, McGregor et al. 2004; Carrasco et al. 2012) commissioning at the end of 2012 marked the installation of the first facility MCAO system at an 8m telescope. Two deformable mirrors in GeMS/GSAOI are conjugated to turbulence in the ground layer and at 9 km altitude, respectively. The system has been in full science operation since then. Similar technology is currently tested at the Large Binocular Telescope (LBT) with LINC-NIRVANA (Herbst et al. 2016). Other multiple guide star AO systems currently in preparation, and correcting the ground layer only, are LBT/ARGOS (Orban de Xivry et al. 2016) and VLT/GRAAL+GALACSI (Kolb et al. 2016).

* E-mail: mschirme@gemini.edu

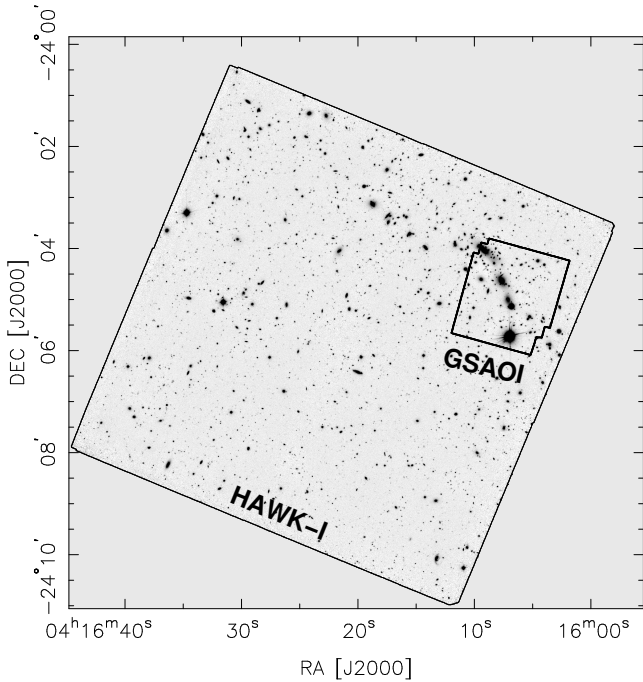


Figure 1. Sky positions of the two comparison data sets.

Of the 116 proposals accepted for GeMS/GSAOI in semesters 2013A through 2017A, 63 per cent have their focus on galactic targets, and 20 per cent on nearby (i.e. well-resolved, angular diameters $\gtrsim 10''$) extragalactic sources. The remaining 17 per cent aim at distant galaxies with angular diameters comparable to the natural seeing disk and below. The strong focus on galactic sources is partially driven by the availability of suitably bright ($R < 15.5$ mag) NGS asterisms, often absent at high galactic latitudes.¹

For the galactic and nearby extragalactic targets, the focus with GeMS/GSAOI is mostly on resolved stellar populations (e.g. Bernard et al. 2016) and proper motions (e.g. Massari et al. 2016; Fritz et al. 2017); in other words, the photometry and location of point sources. The majority of these programs aims at bright targets, often against a crowded background, with typical exposure times of 0.1 – 1 hour per filter. The performance of GeMS/GSAOI in this area is well understood (e.g. Rigaut et al. 2014; Neichel et al. 2014a,b; Turri et al. 2015; Dalessandro et al. 2016).

Much less well investigated is the gain for the remaining 17 per cent of MCAO programs focusing on distant galaxies (e.g. Schirmer et al. 2015; Sweet et al. 2017). A study about the recovery of morphological parameters of distant galaxies was done by Neichel et al. (2014c). It is based on simulated images (Sérsic profiles), convolved with a spatially dependent model of the GeMS point spread function (PSF). An analysis based on real data is still pending.

In this paper we perform a direct comparison between near diffraction limited images and seeing limited images of the same field obtained with GeMS/GSAOI and

¹ An upgrade to the GeMS NGS wavefront sensors is projected for 2018. With a brightness limit of $R \sim 18$ mag, sky coverage will improve at all galactic latitudes.

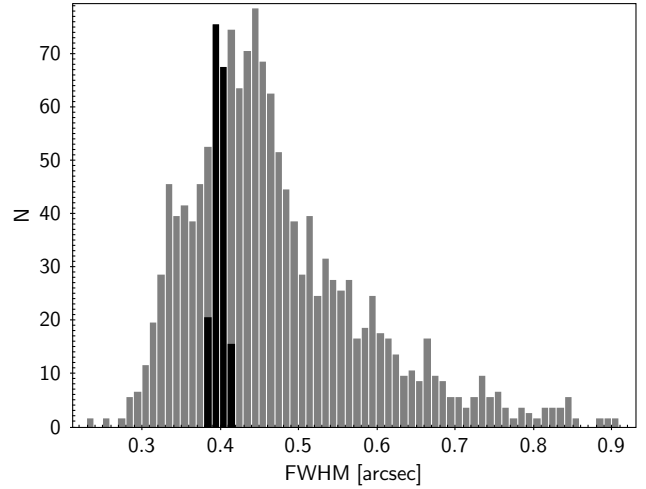


Figure 2. FWHM image seeing of the *full* HAWK-I data set of MACS J0416.1–2403. The comparison image we use in this paper was constructed from a subset of 178 exposures with a seeing of $0''.387\text{--}0''.413$ (black histogram bars).

VLT/HAWK-I, respectively. We measure the gain in depth and signal-to-noise (S/N) in the MCAO data of distant galaxies compared to the natural seeing images.

Our work is organized as follows: Section 2 summarizes the instrumental characteristics of GSAOI and HAWK-I, the observations and data reduction. We analyze the images in Section 3, and present our conclusions in Section 4.

2 OBSERVATIONS AND DATA REDUCTION

2.1 Gemini/GSAOI and VLT/HAWK-I

The focal plane of GSAOI (McGregor et al. 2004; Carrasco et al. 2012) is formed by a 2×2 mosaic of Hawaii 2RG detectors with 2048×2048 pixel each; the gaps between the detectors measure $2''.8\text{--}3''.0$. The native pixel scale varies smoothly between $0''.0194\text{--}0''.0199$, and the field of view is $85'' \times 85''$. The diffraction limit of the Gemini South telescope is 55 milli-arcsec (mas) in the K_s -band; with optimal NGS configurations and good laser return from the atmospheric sodium layer, a resolution of 60 mas has been obtained.

Like GSAOI, the focal plane of HAWK-I (Pirard et al. 2004; Casali et al. 2006; Kissler-Patig et al. 2008; Siebenmorgen et al. 2011) consists of a 2×2 mosaic of Hawaii 2RG detectors. The pixel scale is $0''.1064$, a factor of five larger than for GSAOI, and the detector gaps are $15''$ wide. HAWK-I covers a $7''.5 \times 7''.5$ field of view.

The comparison in this paper is facilitated by the instruments' similar characteristics. Both cameras use the same NIR detector type and are mounted at telescopes with $\sim 8m$ apertures at similar altitudes (2700m for Gemini South, 2600m for the VLT). The telescopes are located in Chile, where they experience similar large-scale weather systems. Nonetheless, the local weather can differ substantially at any given time. This, however, can be ignored for the purposes of this paper, as both data sets were taken in very good conditions.

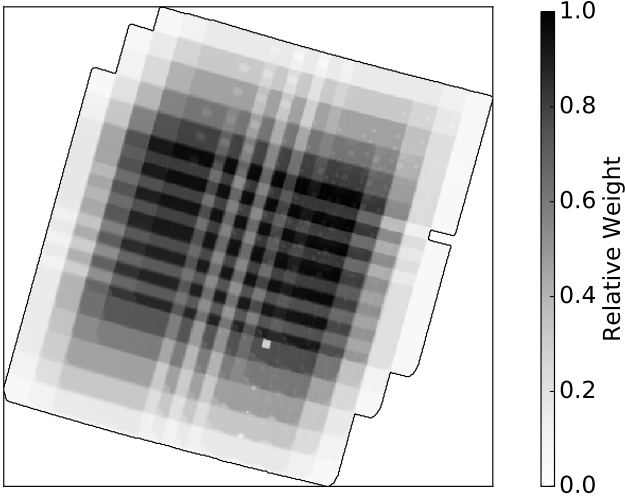


Figure 3. Normalized weight map of the coadded GSAOI image, showing the uneven depth of the data. The *total* integration time is 16 ks, the *average* exposure time is that of 10 ks.

2.2 Observations

The GSAOI data were obtained under Gemini programme GS-2013B-DD-1 (PI Carrasco) on five nights in January 2014, totaling 184×120 s. Exposures with inferior corrected seeing (one night with bad natural seeing) were rejected, resulting in a total integration time of 15720 s. The comparison in this work is based on the publicly released coadded image `MACS_J0416.1-2403_GSAOI_0.02_deep.fits` (see table 3 in Schirmer et al. 2015), which is available online².

The HAWK-I data were obtained under ESO programme 092.A-0472 (Brammer et al. 2016) on 28 nights between October 2013 and February 2014, totaling 1740×56 s. Each 56 s exposure is constructed from 8 s images, averaged using on-detector computations before readout. 178 exposures were selected to construct the natural seeing image for our comparison; details about the selection are provided below.

In both data sets, the sensitivity for all exposures is limited by thermal background.

2.3 Data reduction

All data were reduced using THELI (Schirmer 2013; Erben et al. 2005). Processing of the HAWK-I data followed NIR standard procedures including flat-fielding, dynamic two-pass background modeling, astrometric calibration against 2MASS (Skrutskie et al. 2006), distortion correction, adjustment of relative photometric zeropoints to compensate for variable atmospheric transmission, and finally a weighted image coaddition.

The GSAOI data were processed similarly. Full details are given in Schirmer et al. (2015), with emphasis on astrometric correction and background subtraction. The images were registered against an astrometric reference grid con-

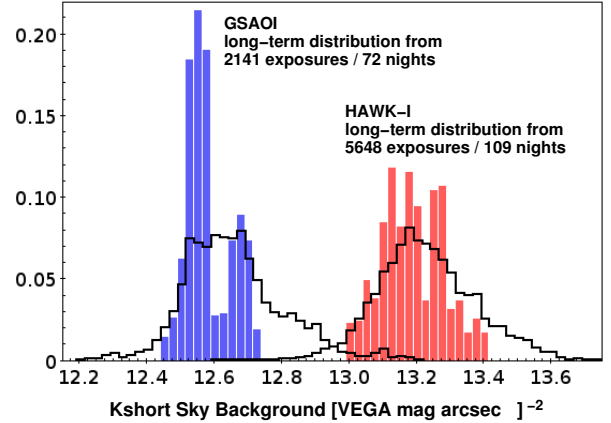


Figure 4. Observed K_s thermal background for GSAOI (blue) and HAWK-I (red), irrespective of airmass. The additional contribution from the MCAO unit is evident, as the K_s sky background on Cerro Paranal (VLT) and Cerro Pachon (Gemini) are within 0.1 mag, otherwise. The blue and red histograms show the background distributions for the exposures that were used for the coadded images. The solid lines display the long-term distributions seen by both instruments between years 2013 and 2015; the data for our comparison were taken in representative conditions.

structed from the sources in the coadded HAWK-I image. Thus, both data sets share the same world coordinate grid.

2.4 Construction of the comparison images

For our comparison to be meaningful, the two coadded images should be built from images with stable seeing, and have the same effective exposure time and PSF sampling. Thanks to the large number of HAWK-I images we could easily select a sub-sample meeting these criteria:

The image quality of the GSAOI data is $0''.08-0''.10$ (the natural seeing was $0''.4-0''.9$). From the HAWK-I data, 178 exposures were selected with a seeing of $0''.387-0''.413$ (Fig. 2), yielding a total exposure time of 9968 s. This is lower than the total exposure time for GSAOI (16 ks). However, the GSAOI data are widely dithered and the detector gaps add to the non-uniformity of the effective exposure time (Fig. 3); the *average* depth is that of 10 ks. The GSAOI data fully fit into one HAWK-I detector, and the HAWK-I exposure time is uniform across that area (see Fig. 1). Lastly, the sampling of the coadded images is also similar. There are 4.2 pixels in the full width half maximum (FWHM) of the GSAOI image ($0''.085$ seeing), and 3.9 pixels in the FWHM of the HAWK-I image ($0''.41$ seeing).

Note that the natural seeing of the HAWK-I exposures selected for the analysis is narrowly clustered around $0''.4$, whereas the GeMS/GSAOI data have a natural seeing of $0''.4-0''.9$. If the focus of the analysis was more on the actual difference brought by GeMS, then one should select the HAWK-I images such that their seeing distribution resembles that of the GeMS/GSAOI data. This, however, is not the scope of our work.

² <http://www.gemini.edu/node/12254>

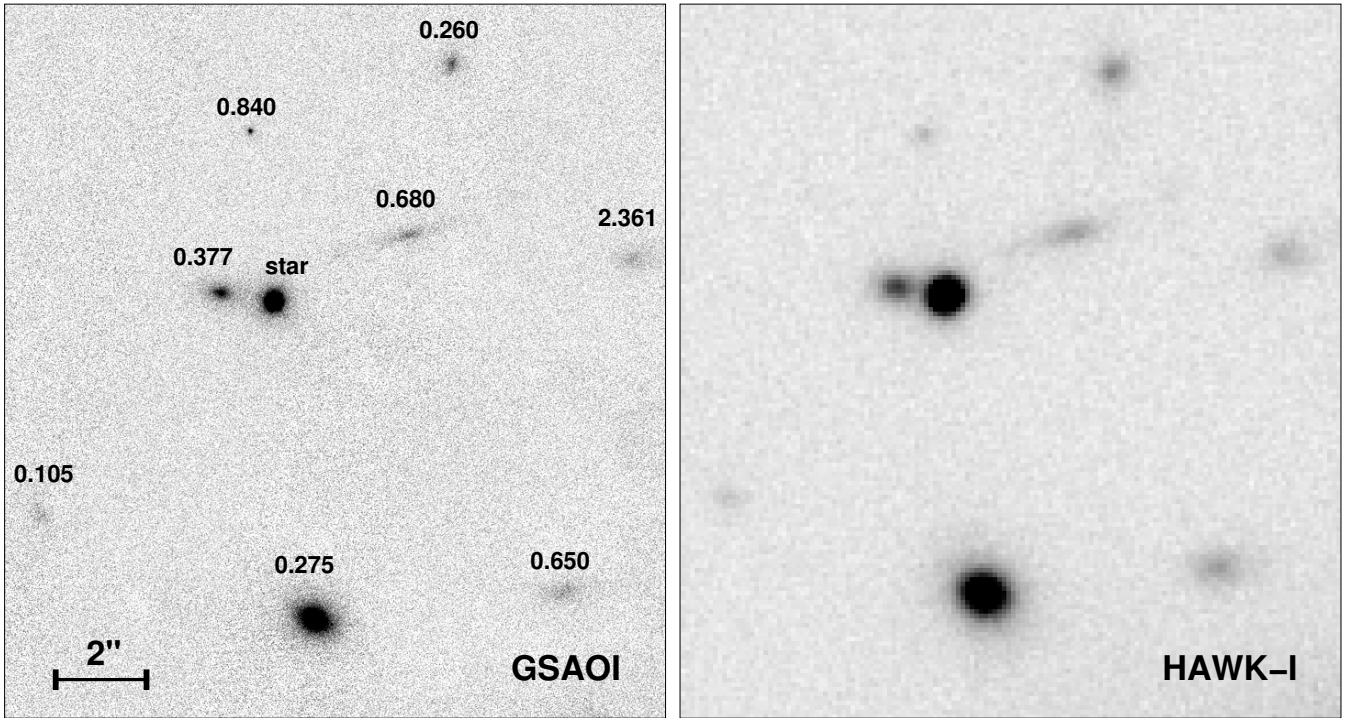


Figure 5. Images of distant galaxies as seen by GSAOI (left, including photometric redshifts of [Castellano et al. 2016](#)) and HAWK-I (right, 5 times enlarged). The detection limit for the blurred HAWK-I data is mostly independent of the intrinsic source profiles.

3 ANALYSIS

3.1 Reduced throughput and enhanced thermal background from MCAO

An important difference between HAWK-I and GeMS/GSAOI is that GeMS adds one transmissive and eight reflective elements to the optical path. The total throughput (telescope to detector) in K_s -band for GSAOI is 31 per cent ([Rigaut et al. 2014](#)). In comparison, for HAWK-I we have a total *instrument* throughput of $\gtrsim 50$ per cent ([Kissler-Patig et al. 2008](#)). The typical reflectivity of the VLT’s aluminum-coated mirrors is 0.97 in K_s -band ([Ettliger et al. 1999](#)), and there are three mirrors in front of HAWK-I (which is mounted at the Nasmyth focus). Hence we estimate the total net throughput to ~ 45 per cent. This is significantly more than the 31 per cent for GeMS/GSAOI, and can be explained if the eight mirrors in GeMS, and the science fold and AO fold flat mirrors (all silver coated) have a mean reflectivity of 0.97. Nominally, silver has a reflectivity of 0.980 – 0.985 in K_s -band, and perhaps it degraded since the commissioning of the system (no measurement data available). We conclude that the MCAO system removes about 0.4 mag sensitivity mainly because of the higher number of optical surfaces.

GeMS is kept at ambient temperature, increasing the thermal background seen by GSAOI. The average long-term K_s background for GSAOI is 12.6 ± 0.2 VEGA mag arcsec $^{-2}$, compared to 13.2 ± 0.2 mag arcsec $^{-2}$ measured by Gemini/FLAMINGOS-2 (a NIR imaging spectrograph,

which does not have the MCAO system in its path)³. Our MCAO system therefore adds ~ 0.6 mag to the sky brightness in K_s , implying 1.7 times longer integration times to reach the same S/N. This is a bit lower than the commissioning results from [Carrasco et al. \(2012\)](#), who determined the instrumental contribution of GeMS by observing blank sky fields once through the AO system, and once by bypassing it. They find factors of 1.5 – 3.5 or, averaged over the K_s bandpass, a thermal contribution of 0.9 mag. The difference to 0.6 mag measured by our long-term data is not surprising, given the high susceptibility of the K_s background to ambient temperature. For example, our long-term FLAMINGOS-2 statistics shows that the K_s background at Gemini South increases by 0.05 mag for every degree of the primary mirror temperature. Together, these are strong arguments for cooled (yet non-cryogenic) MCAO systems such as NFIRAOS ([Herriot et al. 2010](#)) at the Thirty Meter Telescope, and high altitude sites that provide a generally colder climate.

Figure 4 shows the combined instrumental and sky background for GSAOI and HAWK-I, together with their long-term distributions. The latter were measured from archival images, showing that both data sets were obtained in typical conditions. The background seen by HAWK-I (13.2 ± 0.2 mag arcsec $^{-2}$) is the same as that of FLAMINGOS-2, i.e. Cerro Paranal (VLT) and Cerro Pachon (Gemini) share the same K_s -band sky brightness.

Because of the reduced throughput and increased background, GeMS/GSAOI lose 1.0 mag compared to a seeing

³ The FLAMINGOS-2 statistics will be published elsewhere.

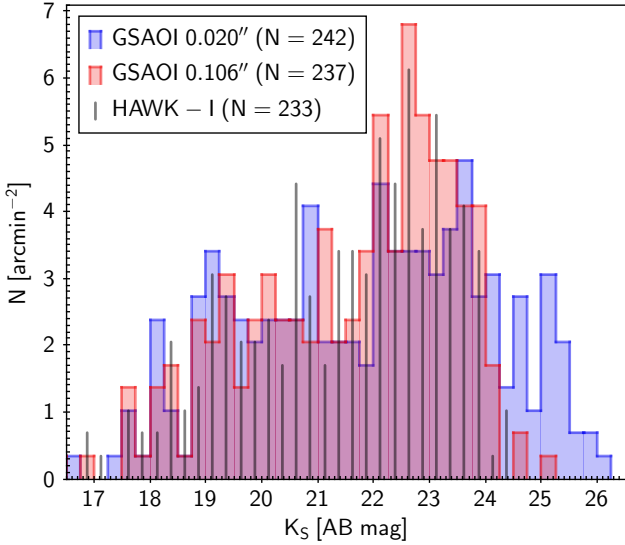


Figure 6. Number counts for the HAWK-I (vertical lines) and GSAOI stacks, once for the native GSAOI pixel scale (blue histogram), and once for the GSAOI data resampled to the HAWK-I pixel scale (red histogram). The counts were measured in the area common to both data sets (see Fig. 1). Down to $K_s \sim 22.5$ (completeness limit) the counts are similar, below that we detect more sources with GSAOI. Further details are given in the main text.

limited instrument such as HAWK-I. In the rest of this paper, we quantify how much GeMS compensates for this loss, because it concentrates the light of distant galaxies in a smaller area with lower cumulative sky noise. This depends on the intrinsic sizes and morphologies of these galaxies, and is best studied with real data. Typical background galaxies with redshifts $z \gtrsim 1$ have sizes of $0''.10$ – $0''.25$ (as resolved by the Hubble Space Telescope, see Roche et al. 1996; Schmidt et al. 2012). This is 2 – 4 times smaller than the PSF of our HAWK-I image, and hence these objects should respond particularly well to MCAO.

3.2 Number counts

One way to compare the images are number counts. The interpretation is not straight forward though, because most distant galaxies have angular diameters smaller than the natural seeing. Once convolved by the natural seeing PSF, the galaxy images have approximately the same size (Fig. 5) and respond uniformly to the detection filters. The detection limit in MCAO data, on the other hand, depends on the sources’ light profiles. A faint and compact object may easily be detected in the MCAO data, but not in a classical image. Likewise, each pixel of an extended low surface brightness galaxy could be pushed below the detection threshold in MCAO data (because its light is distributed over many pixels), yet it would be detected in the classical data with larger pixel scale.

We probe these effects using two different coadditions of the GSAOI data, once maintaining the native plate scale of $0''.02$ pixel $^{-1}$, and once resampling to the HAWK-I plate scale of $0''.106$ pixel $^{-1}$. Object detection is done on all three images (the two GSAOI versions, and the reference HAWK-I

image) with **SExtractor** (Bertin & Arnouts 1996). Detection thresholds of `DETECT_THRESH` = 2.0 and `DETECT_MINAREA` = 4 are applied, i.e. an object must consist of at least 4 connected pixels with $S/N \geq 2$ each. Coadded weight maps are used to take local noise properties into account. HAWK-I detections are considered only if they fall within the GSAOI field of view (Fig. 1), avoiding biases by the strong concentration of cluster galaxies.

The results are shown in Fig. 6. The turn-over point (completeness limit) is reached at $K_s \sim 22.8$ AB mag in the HAWK-I and the rebinned GSAOI image, with approximately equal counts at brighter magnitudes. Overall, the count profile for the HAWK-I image (vertical lines) and the rebinned GSAOI image (red histogram) are very similar. For fainter magnitudes, more detections are being made in the GSAOI data, in particular the one with the native pixel scale. We conclude that the wavefront correction fully makes up for the loss in overall throughput and the enhanced background of the MCAO.

The histograms in Fig. 6 reveal that the effective 5-fold rebinning lifts pixels below the 2σ detection threshold in the unbinned image over the threshold in the binned image. Consequently, objects in the unbinned image and with magnitudes 24 – 26 (blue histogram) become 1 – 1.5 mag brighter, which is seen in the higher number counts around 23 – 24 mag (red histogram). However, the binning also concentrates more sky noise into the measurement aperture, and thus the very faint and smallest objects are lost compared to the unbinned image.

Our analysis verifies that the light profiles of compact galaxies affect their response to the detection filters in near diffraction limited images. The depth of a MCAO image is therefore no longer a simple function of magnitude as in a seeing limited image, and the concept of “limiting magnitude” is less well defined. A more robust analysis of the number counts is prohibited by the low number of detections, and would require to go about half a magnitude deeper for this particular target area.

3.3 Direct S/N comparison

A better and more direct way to quantify the gain by MCAO is to compare the S/N of individual sources. We use the **SExtractor** catalogs from Sect. 3.2 for the unbinned GSAOI image and the HAWK-I image. Only sources that are common to both catalogs enter the analysis.

The background noise in the GSAOI image is uneven (Sect. 2.4). We must therefore estimate the S/N an individual source would have if it did not fall into an area with increased noise. We extract relative correction factors from the coadded weight image (Fig. 3), which reflects the noise characteristics ($\text{weight} \propto \text{noise}^{-2}$).

We then calculate $(S/N_{\text{GSAOI}}) / (S/N_{\text{HAWK-I}})$ for stars and galaxies, i.e. the *ratio of S/N*. It is shown as a function of the half-light radius r_h (**SExtractor**’s `FLUX_RADIUS`) and magnitude in Fig. 7. We use r_h instead of FWHM because it is less susceptible to substructure. The image seeing of HAWK-I is $r_h = 0''.26 \pm 0''.01$. For sources larger than the seeing disk there no gain is detected (as expected). Sources with intrinsic sizes of about half the seeing value gain ~ 40 per cent in S/N. Even smaller sources experience a substantial boost by factors of 2.0 – 2.5. Note that this performance

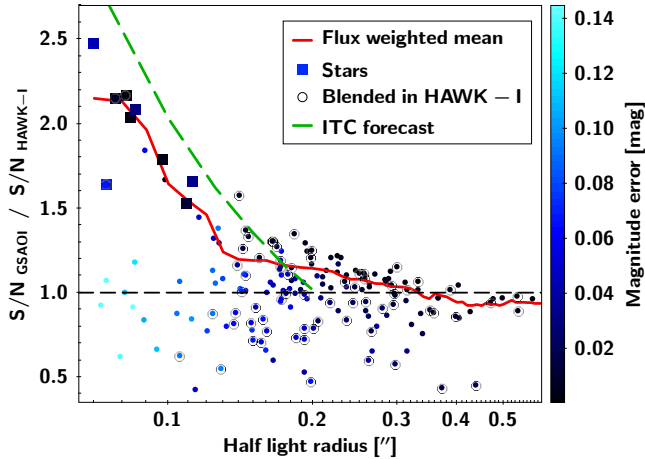


Figure 7. Ratio of S/N between GSAOI and HAWK-I as a function of the source half-light radius and magnitude. The HAWK-I image seeing has a measured half-light radius of $0''.26$. Sources with intrinsic diameters of half the natural seeing disk already gain ~ 40 per cent in S/N from MCAO. Even smaller sources experience a dramatic boost. Sources which are blended in the HAWK-I data and resolved by GSAOI are marked with open circles. They appear to have less gain in S/N because the combined flux in HAWK-I is compared with the (reduced) flux of the closest GSAOI detection. The dashed green line is the prediction from a comparison of the GSAOI and HAWK-I integration time calculators.

boost is conservative, because only a single NGS was available, resulting in $0''.072$ near the guide star and $0''.122$ at the largest separation (see Schirmer et al. 2015). With a better NGS configuration we would have reached $0''.06 - 0''.07$ over the entire field, improving the S/N further and for more sources.

Figure 7 also reveals objects for which the MCAO correction appears to reduce the S/N. 60 – 65 per cent of those are blended in the HAWK-I data and resolved by GSAOI. The resolved component in GSAOI that is matched with the blended HAWK-I source has systematically lower flux. There is also a clear trend with magnitude error: sources with higher flux are less impacted by noise, therefore the gain by MCAO is more readily visible.

We also overplot a theoretical prediction (dashed green line in Fig. 7), using the GSAOI and HAWK-I integration time calculators (ITC). The prediction is limited because of the inherent limitations of these tools. We use a source with $K_s = 24$ VEGA mag and a spectrum of an elliptical galaxy mapped to redshift 1.0. The magnitude is irrelevant because we build the ratio of S/N, and so is the type of the spectrum because the relative response of both instruments across the K_s band is similar.

For the HAWK-I ITC, we use a point source (always smaller than $0''.4$), a fixed ($0''.4$) image FWHM at an airmass of 1.2, and 1246 exposures with 8s DITs (detector integration time, reflecting the total of 9968s). The same is done for the GSAOI ITC, but with 83×120 s exposures, and calculations for a range of FWHM for an extended Gaussian source profile. The FWHM are converted to half-light radii, and the GSAOI S/N is normalized by the S/N for HAWK-I. The prediction breaks down for FWHM equal or larger than

the HAWK-I seeing, because then our assumption of a point source in the HAWK-I ITC is no longer valid. Overall, the prediction is fairly good over its valid range.

4 SUMMARY

We compared a unique set of observations of the same extragalactic target, obtained with two of the most advanced NIR imagers currently available at 8m telescopes: GeMS/GSAOI at the Gemini South telescope, and HAWK-I at the VLT. We quantified the performance gain delivered by MCAO over classical imaging for distant galaxies, as a function of their intrinsic size and magnitude, and compared with the prediction from integration time calculators.

This is the first study of this kind based on real data, and it is quite unique. We are using a set of K_s -band images of the *Frontier Field* galaxy cluster MACS J0416.1–2403. No other target has been observed as deep as this one with GeMS/GSAOI (MCAO); simultaneously, it is also one of the deepest observations that have been conducted with VLT/HAWK-I (classical imaging). To date, this is *the only* existing matching pair of sufficiently deep observations to evaluate the performance gain of MCAO for distant extragalactic targets with real data. Our results are as follows:

- (i) The MCAO of GeMS causes a nominal 1.0 mag loss in sensitivity in K_s -band because of reduced throughput (0.4 mag; additional optical surfaces) and increased thermal background (0.6 mag; ambient temperature).
- (ii) The wavefront correction concentrates the light of the distant galaxies into smaller apertures with less cumulative sky noise. Our number counts show that this fully compensates for the loss in throughput and enhanced sky background.
- (iii) MCAO starts to improve the S/N of individual sources once their intrinsic diameters become smaller than the natural seeing. Sources half the size of the seeing disk already gain ~ 40 per cent. Below this, the improvement in S/N is dramatic, reaching factors 2 – 2.5 for the smallest and most distant galaxies.
- (iv) The integration time calculators (ITCs) predict the gain in S/N with useful accuracy, although slightly optimistic for GeMS. The latter is at least to some extent caused by our imperfect NGS constellation that cannot be reflected in the ITC.

The performance gain we measured is a conservative lower limit. The field of MACS J0416–2403 offered only one natural guide star for tip-tilt and focus correction, preventing to reach the best image quality across the entire field of view. With an optimal NGS constellation (3 stars in a wide triangular fashion), we would have achieved 20 – 50 per cent better image quality across the field.

We recognize the limited statistics for our analysis. The field of view of GSAOI is comparatively small, and we do not reach as deep as the *full* HAWK-I data set. A larger survey area, and/or deeper observations with GSAOI, would have resulted in a larger number of common sources and a clearer result for the number counts analysis. Such data do not yet exist, but with other MCAO systems on the horizon and the coming upgrades to GeMS (new laser and wave front sensors) this is hopefully just a matter of time.

Lastly, we wish to emphasize the importance of future cooled (non-cryogenic) MCAO systems with high optical throughput. They should result in a significant performance gain, reducing the gap between ground-based observatories and the future James Webb Space Telescope.

ACKNOWLEDGMENTS

The authors thank the referee, Francois Rigaut, for his comments that substantially improved the readability and accuracy of this manuscript. Author contributions: MS reduced and analyzed both data sets and wrote the manuscript. GS and VG maintain and improve GeMS, and operate it at night together with EM. RC lead the proposal for the GSAOI data.

Based on observations obtained at the Gemini Observatory, which is operated by the Association of Universities for Research in Astronomy, Inc., under a cooperative agreement with the NSF on behalf of the Gemini partnership: the National Science Foundation (United States), the National Research Council (Canada), CONICYT (Chile), Ministerio de Ciencia, Tecnología e Innovación Productiva (Argentina), and Ministério da Ciência, Tecnologia e Inovação (Brazil).

Based on observations made with the European Southern Observatory under Program 092.A-0472(A), Chile.

REFERENCES

- Bernard A., Neichel B., Samal M. R., Zavagno A., Andersen M., Evans C. J., Plana H., Fusco T., 2016, *A&A*, **592**, A77
- Bertin E., Arnouts S., 1996, *A&AS*, **117**, 393
- Brammer G. B., et al., 2016, preprint, ([arXiv:1606.07450](https://arxiv.org/abs/1606.07450))
- Carrasco E. R., et al., 2012, in Society of Photo-Optical Instrumentation Engineers (SPIE) Conference Series. , [doi:10.1117/12.926240](https://doi.org/10.1117/12.926240)
- Casali M., et al., 2006, in Society of Photo-Optical Instrumentation Engineers (SPIE) Conference Series. p. 62690W, [doi:10.1117/12.670150](https://doi.org/10.1117/12.670150)
- Castellano M., et al., 2016, *A&A*, **590**, A31
- Dalessandro E., et al., 2016, *ApJ*, **833**, 111
- Ellerbroek B., Rigaut F., 2000, *Nature*, **403**, 25
- Erben T., Schirmer M., Dietrich J., et al., 2005, *AN*, **326**, 432
- Ettliger E., Giordano P., Schneermann M., 1999, *The Messenger*, **97**, 4
- Fritz T. K., et al., 2017, *ApJ*, **840**, 30
- Herbst T. M., Ragazzoni R., Bertram T., Bizenberger P., Briegel F., Hofferbert R., Kürster M., 2016, in Ground-based and Airborne Instrumentation for Astronomy VI. p. 99080N, [doi:10.1117/12.2232707](https://doi.org/10.1117/12.2232707)
- Herriot G., et al., 2010, in Adaptive Optics Systems II. p. 77360B, [doi:10.1117/12.857662](https://doi.org/10.1117/12.857662)
- Kissler-Patig M., et al., 2008, *A&A*, **491**, 941
- Kolb J., et al., 2016, in Adaptive Optics Systems V. p. 99092S, [doi:10.1117/12.2232788](https://doi.org/10.1117/12.2232788)
- Massari D., et al., 2016, *A&A*, **586**, A51
- McGregor P., et al., 2004, *Proc. SPIE*, **5492**, 1033
- Melnick J., Marchetti E., Amico P., 2012, in Adaptive Optics Systems III. p. 84470M, [doi:10.1117/12.925185](https://doi.org/10.1117/12.925185)
- Neichel B., Lu J. R., Rigaut F., Ammons S. M., Carrasco E. R., Lassalle E., 2014a, preprint, ([arXiv:1409.0719](https://arxiv.org/abs/1409.0719))
- Neichel B., et al., 2014b, *MNRAS*, **440**, 1002
- Neichel B., Huertas-Company M., Huellou T., Epinat B., Puech M., Gratadour D., 2014c, in Adaptive Optics Systems IV. p. 91484O, [doi:10.1117/12.2055326](https://doi.org/10.1117/12.2055326)
- Orban de Xivry G., et al., 2016, in Adaptive Optics Systems V. p. 990936, [doi:10.1117/12.2240094](https://doi.org/10.1117/12.2240094)
- Pirard J.-F., et al., 2004, in Moorwood A. F. M., Iye M., eds, *Proc. SPIE Vol. 5492, Ground-based Instrumentation for Astronomy*. pp 1763–1772, [doi:10.1117/12.578293](https://doi.org/10.1117/12.578293)
- Ragazzoni R., Marchetti E., Valente G., 2000, *Nature*, **403**, 54
- Rigaut F., et al., 2014, *MNRAS*, **437**, 2361
- Roche N., Ratnatunga K., Griffiths R. E., Im M., Neuschaefer L., 1996, *MNRAS*, **282**, 1247
- Schirmer M., 2013, *ApJS*, **209**, 21
- Schirmer M., Carrasco E. R., Pessev P., Garrel V., Winge C., Neichel B., Vidal F., 2015, *ApJS*, **217**, 33
- Schmidt F., Leauthaud A., Massey R., Rhodes J., George M. R., Koekemoer A. M., Finoguenov A., Tanaka M., 2012, *ApJ*, **744**, L22
- Siebenmorgen R., Carraro G., Valenti E., Petr-Gotzens M., Brammer G., Garcia E., Casali M., 2011, *The Messenger*, **144**, 9
- Skrutskie M. F., et al., 2006, *AJ*, **131**, 1163
- Sweet S. M., et al., 2017, *MNRAS*, **464**, 2910
- Turri P., McConnachie A. W., Stetson P. B., Fiorentino G., Andersen D. R., Véran J.-P., Bono G., 2015, *ApJ*, **811**, L15

This paper has been typeset from a $\text{\TeX}/\text{\LaTeX}$ file prepared by the author.